



HAL
open science

Relationship between the carbon nano-onions (CNOs) surface chemistry/defects and their capacitance in aqueous and organic electrolytes

Georges Moussa, Camélia Matei Ghimbeu, Pierre-Louis Taberna, Patrice Simon, Cathie Vix-Guterl

► To cite this version:

Georges Moussa, Camélia Matei Ghimbeu, Pierre-Louis Taberna, Patrice Simon, Cathie Vix-Guterl. Relationship between the carbon nano-onions (CNOs) surface chemistry/defects and their capacitance in aqueous and organic electrolytes. *Carbon*, 2016, vol. 105, pp. 628-637. 10.1016/j.carbon.2016.05.010 . hal-01466641

HAL Id: hal-01466641

<https://hal.science/hal-01466641>

Submitted on 13 Feb 2017

HAL is a multi-disciplinary open access archive for the deposit and dissemination of scientific research documents, whether they are published or not. The documents may come from teaching and research institutions in France or abroad, or from public or private research centers.

L'archive ouverte pluridisciplinaire **HAL**, est destinée au dépôt et à la diffusion de documents scientifiques de niveau recherche, publiés ou non, émanant des établissements d'enseignement et de recherche français ou étrangers, des laboratoires publics ou privés.



Open Archive TOULOUSE Archive Ouverte (OATAO)

OATAO is an open access repository that collects the work of Toulouse researchers and makes it freely available over the web where possible.

This is an author-deposited version published in : <http://oatao.univ-toulouse.fr/>
Eprints ID : 16654

To link to this article : DOI:10.1016/j.carbon.2016.05.010
URL : <http://dx.doi.org/10.1016/j.carbon.2016.05.010>

To cite this version : Moussa, Georges and Matei Ghimbeu, Camélia and Taberna, Pierre-Louis and Simon, Patrice and Vix-Guterl, Cathie *Relationship between the carbon nano-onions (CNOs) surface chemistry/defects and their capacitance in aqueous and organic electrolytes*. (2016) Carbon, vol. 105. pp. 628-637. ISSN 0008-6223

Any correspondence concerning this service should be sent to the repository administrator: staff-oatao@listes-diff.inp-toulouse.fr

Relationship between the carbon nano-onions (CNOs) surface chemistry/defects and their capacitance in aqueous and organic electrolytes

Georges Moussa^{a, b, c}, Camélia Matei Ghimbeu^{a, c, *}, Pierre-Louis Taberna^{b, c},
Patrice Simon^{b, c}, Cathie Vix-Guterl^{a, c}

^a Institut de Science des Matériaux de Mulhouse (IS2M), UMR CNRS 7361, Université de Haute Alsace, 15 rue Jean Starcky, 68057 Mulhouse, France

^b Centre Interuniversitaire de Recherche et d'Ingénierie des Matériaux (CIRIMAT), UMR CNRS 5085, Université Paul Sabatier, 118 route de Narbonne, 31062 Toulouse, France

^c Réseau sur le Stockage Electrochimique de l'énergie (RS2E), FR CNRS 3459, 33 Rue Saint Leu, 80039 Amiens Cedex, France

A B S T R A C T

The effect of surface functionalities on the supercapacitors performances has been highlighted often in many works. However, studies devoted to the influence of carbon defects did not gain particular attention due to the difficulty to quantify such parameter. In this context, carbon nano-onions were used as model material in order to understand the influence of the surface chemistry (nature and amount of oxygen groups) and structural defects (active surface area, ASA) on the capacitance. Different types of thermal treatments in oxidizing or reducing atmospheres allowed to finely tune the surface chemistry and the ASA as demonstrated by temperature programmed desorption coupled with mass spectrometry (TPD-MS). For the first time, the precise control of these characteristics independently one of each other allowed to highlight an important influence of the carbon defects on the capacitance in organic and aqueous electrolytes which outbalance the oxygen functional group effect.

1. Introduction

During the past years, important scientific and industrial developments have led to an extensive development of supercapacitors as electrochemical energy storage devices. Supercapacitors are environmentally friendly, of high safety and can be operated in a wide temperature range with a near-infinite long cycling life [1]. They exhibit high power density, which explains their utilization in many applications requiring energy pulses during short periods of time (automobiles, tramways, buses, wind turbines etc) [2]. Depending on the charge storage mechanism, two types of supercapacitors can be defined [3]: EDLC (electrical double layer capacitors) and redox-based electrochemical capacitors [4–7]. In the first one, the charge is stored by reversible electrostatic adsorption of ions at high surface area electrode/electrolyte

interface [8] while in redox-based electrochemical capacitors the storage is achieved through faradic processes [9]. In a first approach, energy density in EDLC is proportional to the electrode accessible surface area and therefore the electrode materials with large porous volume and high surface area are required [1]. Owing to their low cost, chemical stability and sustainable origin from natural/abundant sources, carbon materials are the most popular materials employed as electrodes for supercapacitor [3,5,10,11].

Since 2005, several studies have shown that not only the surface area but also the carbon pore size distribution (PSD) and the electrolyte ions size play an important role in carbon capacitance [3,12–21]. It was shown that the capacitance increases when the micropore size distribution approaches the bare electrolyte ions size [12,18]. In some cases, limitation of capacitance was observed due to the saturation of the carbon pores with ions or due to steric (volumetric) effects [19]. Aside, the presence of mesopores facilitates the transport of electrolyte ions, acting as electrolyte reservoir, thereby increasing the access of the electrolyte to the microporosity [22–24]. Therefore, the relationship between the textural properties of porous carbons and the capacitance are well

* Corresponding author. Institut de Science des Matériaux de Mulhouse (IS2M), UMR CNRS 7361, Université de Haute Alsace, 15 rue Jean Starcky, 68057 Mulhouse, France.

E-mail address: camelia.ghimbeu@uha.fr (C. Matei Ghimbeu).

described in the literature for all sorts of electrolytes (aqueous, organic and ionic liquids) [18,25].

Another important parameter known to influence the capacitance is the surface chemistry [26]. The presence of oxygen, sulfur, phosphorus and nitrogen based functional groups [27–29] in the carbon structure/surface leads to improvement of the capacitance through redox reactions with the electrolyte by so-called pseudo-capacitance mechanisms [4,7,30,31]. The presence of oxygen functionalities allows increasing the specific capacitance in aqueous electrolytes [28,29] while it might be detrimental in organic electrolytes, where irreversible redox reactions may take place between the electrolyte and oxygen groups [4,26]. The capacitance is influenced by the nature of oxygen groups (carboxylic, phenols, ethers ...) but also by their amount. Oxidation by thermal treatment under air or by chemical treatments with specific agents (H_2O_2 , HNO_3) led to the increase of the quantity of surface oxygen groups, while heating under inert atmosphere (Ar , H_2) is efficient to selectively remove some of these groups. While the nature of oxygen groups may be assessed by several methods, including X-ray photoelectron spectroscopy (XPS), Fourier transform infrared spectroscopy (FTIR), titration and temperature-programmed desorption coupled with mass spectrometry (TPD-MS) [32–35], the quantification of functional groups in whole carbon material can be accurately determined only by TPD-MS.

Although the effect of surface functionalities groups on capacitance have been many times addressed in the literature and reviewed recently [10], works devoted to further understanding of the effect of carbon defects are scarce. Carbon defects such as dislocation, stacking faults or atom vacancies are mainly located in the edge planes of carbon and constitute the so-called active sites or active surface area (ASA) [36,37]. The ASA is an intrinsic structural characteristic of graphitic carbon materials which can be quantified by oxygen chemisorptions at 300°C followed by TPD-MS to quantify the formed CO and CO_2 groups, as described in detail elsewhere [38]. We have previously shown that the ASA is a key parameter that influences the irreversible capacity of graphitic and hard carbon in lithium and Na ion batteries, respectively [38–40]. However, the influence of the presence of active sites on the electrochemical performances of carbon materials in organic- and aqueous-based supercapacitors has not been yet reported to the best of our knowledge.

In this work, carbon nano-onions (CNOs) were selected as model electrode materials due to their high electrical conductivity, short time charging and high power density [11,41–43]. CNOs exhibit moderate specific surface area ($200\text{--}600\text{ m}^2\text{ g}^{-1}$) [11,43,44] compared to that of activated carbons, but their surface is fully accessible to ion adsorption due to the absence of a porous network inside the particles. In addition, they have a hydrophobic character leading to limited capacitance ($25\text{--}50\text{ F g}^{-1}$) [43,44].

Therefore, due to their hydrophobic nature and their non-porous texture, they were selected in this work as model material in order to understand the influence of surface chemistry and presence of defects on their electrochemical performance in aqueous and organic electrolytes. Several thermal treatments allowed to independently modifying their structure and surface chemistry/defects while keeping similar their porous texture.

This systematic study highlighted a Langmuir correlation between the capacitance and the desorbed quantity of oxygenated groups (DQ) while a linear relationship between the capacitance and ASA was found in organic and aqueous electrolyte. The effect in aqueous electrolytes was more pronounced, and high capacitance of $\sim 95\text{ F/g}$ could be reached for some specific treatments. Nevertheless, a predominant effect of the carbon defects (ASA) on the capacitance is evidenced which outbalance the functional group effect.

2. Experimental section

2.1. CNOs synthesis and modification

Ultra-pure nanodiamonds particles (ADAMAS Nanotechnologies Inc.) with nanodiamonds content $\geq 98\%$ were used as received without any further purification. Polytetrafluoroethylene (PTFE) binder was purchased from Aldrich, with 60wt% suspension in water. Tetraethylammonium tetrafluoroborate (NET_4BF_4) (Acros Organics) was dissolved in acetonitrile (ACN) (Acros Organics, $\text{H}_2\text{O} < 10\text{ ppm}$) to prepare 1.5 M NET_4BF_4 in AN electrolyte. Sulfuric acid (H_2SO_4 , Aldrich) was diluted in deionized water, which was further purified with a milli-Q system (Millipore), to prepare 0.1 M H_2SO_4 aqueous electrolyte.

A standard procedure was used to synthesis CNOs from ultra-high pure nanodiamonds (Nds) particles [44–46]. Typically, Nds were heated during one hour under Ar at 1350°C or vacuum at 1700°C , respectively. The resulting materials are denoted C1350 and C1700. The surface chemistry and the quantity of defects of the as-prepared CNOs materials were modified by thermal treatment under air for 1 h and 2 h respectively, at 470°C for C1350 and 580°C for C1700. The resulting modified CNOs are noted as C1350-Tair, C1350-2Tair and C1700-Tair, C1700-2Tair, respectively. Further thermal annealing under hydrogen at 900°C for 1 h was performed on C1350-Tair and C1700-Tair to remove their oxygen surface groups content and the derived materials were labeled as C1350-Tair-H2 and C1700-Tair-H2. A flowchart (Fig. 1) schematically shows the preparation process of the samples.

2.2. Structural and textural characterization

Thermogravimetric analysis (TGA) measurements were performed with a METTLER TOLEDO TGA851 device under air (100 mL min^{-1}) using a heating rate of $10^\circ\text{C min}^{-1}$ in the temperature range of $25\text{--}700^\circ\text{C}$.

The carbon structure was observed by transmission electron microscopy (TEM, JEOL ARM200F instrument) operating at 200 kV. X-Ray powder diffraction (XRD) data were collected with a Philips X'Pert MPD diffractometer with a $\text{Cu K}_{\alpha 1,2}$ doublet and a flat-plate Bragg–Brentano theta–theta geometry. N_2 adsorption analysis was performed with a Micromeritics ASAP 2420 instrument using N_2 as adsorbate at -196°C . Prior to the analysis, the samples were out-gassed overnight under vacuum at 150°C . BET (Brunauer–Emmett–Teller) specific surface area (SSA) was calculated from the linear plot in the relative pressure range of 0.05–0.3. The pore size distribution was determined using a DFT model.

Qualitative and quantitative measurements of oxygen surface groups content was done by temperature programmed desorption coupled with mass spectrometry as described in details elsewhere [38,47]. Briefly, in a typical measurement, the CNOs are placed in a quartz tube and heated under vacuum up to 950°C with a rate of 2°C min^{-1} . The gases evolved during this step were quantitatively detected by a mass spectrometer. The total amount of each gas released was computed by time integration of the TPD curves.

After this treatment at 950°C for 30 min under high vacuum (10^{-4} Pa), the CNOs surface is considered cleaned and ready to the second step where the active surface area is determined as described in the literature [38]. In summary, the CNOs are exposed to oxygen atmosphere at 300°C during 10 h allowing surface oxygen complexes to be formed. Further thermal treatment up to 950°C was used to decompose oxygenated groups in CO and CO_2 , which were quantified by TPD-MS. Considering the number of moles of desorbed gases and the area of an edge carbon site that chemisorbs an oxygen atom (0.083 nm^2) [38,47], the active surface area, ASA (surface area occupied by the chemisorbed oxygen) can

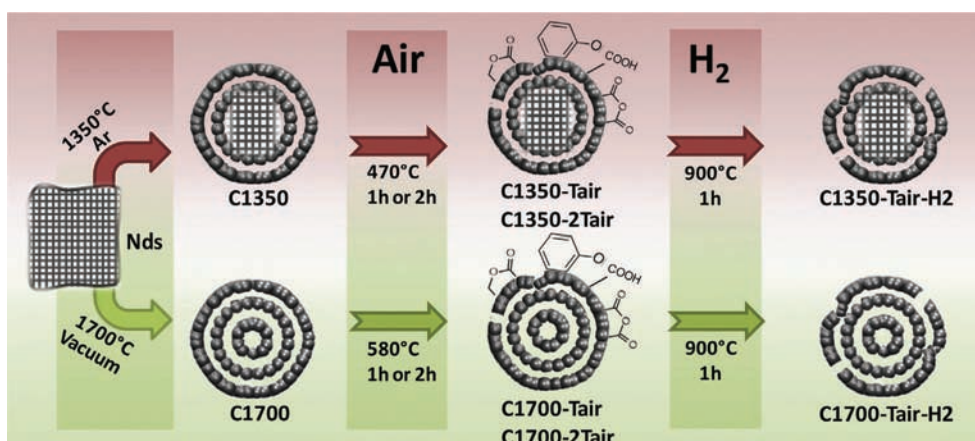


Fig. 1. Flowchart that regroups the different synthesis of CNOs under different thermal treatments. (A color version of this figure can be viewed online.)

be determined.

2.3. Electrochemical characterizations

The CNOs were tested using Swagelok cells in a 2-electrode configuration, by cyclic voltammetry using a multichannel VMP3 potentiostat/galvanostat (Biologic, France). Electrodes were prepared by mixing 95% of CNOs with 5% of polytetrafluoroethylene (PTFE) binder in the presence of ethanol. Electrochemical capacitors were built using two carbon electrodes (8 mm diameter) with comparable mass (~7 mg) and thickness (200 μm) [48] and electrically isolated by a 50 μm -thick porous cellulose as separator disk. The counter electrode was a platinum disk. 0.1 M H_2SO_4 as aqueous electrolyte and 1.5 M $\text{NEt}_4\text{BF}_4/\text{ACN}$ organic electrolyte were used. Cyclic voltammetry was performed in a voltage window between 0 and 0.9 V for aqueous electrolytes and between 0 and 2.5 V for the organic electrolytes at scan rates of 20 mV s^{-1} .

3. Results and discussion

Fig. 2a shows the X-ray diffraction (XRD) patterns of the as received Nds and CNOs obtained at the different annealing temperatures, i.e., 1350 $^\circ\text{C}$ and 1700 $^\circ\text{C}$, respectively.

The XRD pattern of Nds shows an intense peak around 44° (2θ) specific to the (111) interlayer distance, characteristic to sp^3 -bonded carbon with a cubic structural phase (PDF 00-006-0675). For the C1700 sample, an intense peak at around 26° (2θ), characteristic to the (002) interlayer distance, confirms the hexagonal structural phase (sp^2 -bonded carbon, PDF 00-041-1487). However, for the C1350 sample a mix of peaks corresponding to both sp^3 and sp^2 -bonded carbons is observed. The area ratio between the sp^3 (111) and sp^2 (002) peaks decreases from 0.56 to 0.18 when heating from 1350 $^\circ\text{C}$ to 1700 $^\circ\text{C}$. The air oxidation of C1350 (C1350-2Tair) also results in the decrease of the (111)/(002) area peak ratio, from 0.56 for C1350 down to 0.51 for C1350-2Tair (see Fig. S2, Supporting Information). This is explained by the removal of some sp^3 amorphous carbon existing between the particles.

More insights about the structure of Nds and the CNOs were obtained by high-resolution TEM (Fig. 2 a–c). Nds particles present irregular shapes with a crystalline structure (Fig. 2a). When treated at 1350 $^\circ\text{C}$, the morphology changes (Fig. 2b) and the particles become more spherical. We notice that a fraction of particles exhibit a graphitic concentric structure while another part shows a core of un-reacted nanodiamond and a shell of graphitic structure. The ratio between the core and the shell varies with the size of the

particles, i.e., smaller the particles the higher the amount of graphitic shell. This suggests a graphitization process starting from the outer part of the particles. The oxidation process tends to homogenize the particle morphology due to the removal of amorphous carbon necks between the particles; this is particularly visible with the C1350 (see Fig. S2-Supporting Information). For higher annealing temperatures, concentric stacked layers (4–8 shells) of (002) graphitic planes are observed (Fig. 2c), thus confirming the formation of the onion-like structure [44]. The transformation from diamond into graphitic structure is mainly induced by temperature although the annealing atmosphere (Ar for 1350 $^\circ\text{C}$ and vacuum for 1700 $^\circ\text{C}$) may have an influence on the particle morphology/structure [49]. In addition, the transformation of Nds in CNOs is accompanied by an increase of the particle size for ~6 nm for Nds to ~10 nm for C1700, respectively. This is mainly due to the (002) graphitic space layer (~0.34 nm) which is higher than the distance of C–C bond of diamond (0.154 nm).

The surface chemistry and active site amounts of the as-prepared CNOs materials were modified by thermal treatment under air to obtain C1350-Tair and C1700-Tair samples. The two oxidizing temperatures (470 $^\circ$ and 580 $^\circ\text{C}$) were selected on the basis of TGA experiments. The sample weight loss profiles are given in Fig. S1 (Supporting Informations). The C1350 starts to oxidize at around 450 $^\circ\text{C}$ while the onset oxidation temperature of the C1700 was 550 $^\circ\text{C}$. This is related to the different graphitization level as shown by XRD analysis (Fig. 2): the higher the graphitization level (C1700) the lower the reactivity towards oxygen and the higher the oxidation temperature. Because of the reactivity difference in air between the two materials, the same oxidation temperature cannot be used; therefore, a burn-off percentage of ~15% was fixed for both carbons to ensure efficient oxidation treatment but to avoid excessive mass loss during the oxidation.

The textural properties of the as prepared materials and modified ones were determined by nitrogen adsorption/desorption isotherms (Fig. 3). All materials exhibit isotherms with similar shapes and can be classified as type II with a H3 hysteresis loop, characteristic to non-porous materials.

The specific surface area of Nds is 283 $\text{m}^2 \text{g}^{-1}$ and slightly increases up to 294 $\text{m}^2 \text{g}^{-1}$ when treated at 1350 $^\circ\text{C}$. For higher temperatures (1700 $^\circ\text{C}$) the SSA greatly increases up to 437 $\text{m}^2 \text{g}^{-1}$ (see Table 1), in good agreement with other works [50]. The thermal treatment under air induces a significant increase of the SSA of the C1350 material (from 294 to 403 $\text{m}^2 \text{g}^{-1}$), while only a slight increase is noticed for the C1700 sample (from 437 to 501 $\text{m}^2 \text{g}^{-1}$). The increase of the surface area by oxidation is associated with the

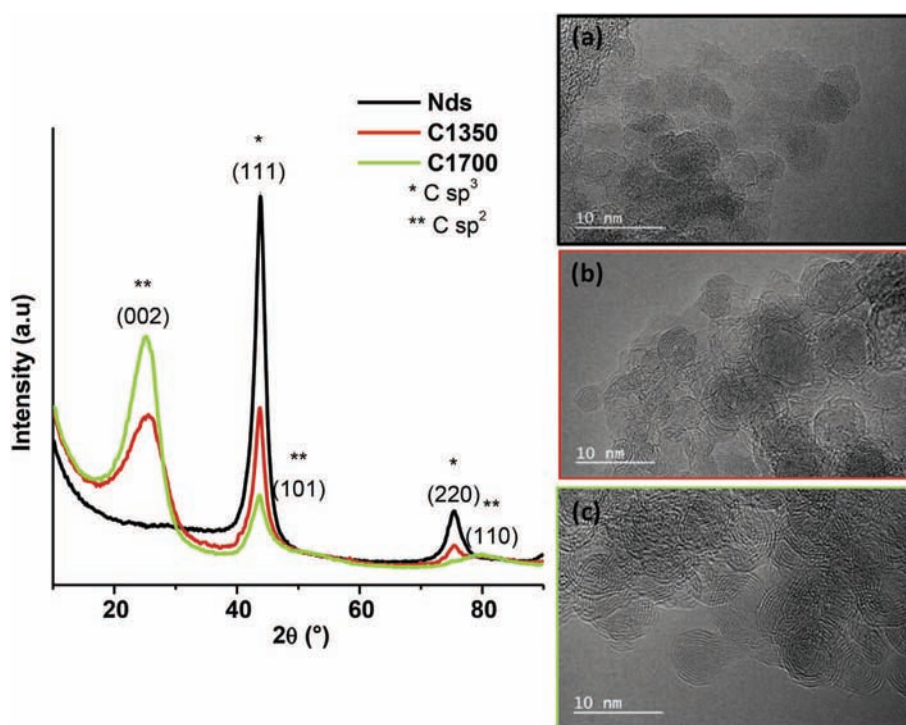


Fig. 2. XRD patterns (left) and HRTEM pictures (right) of a) nanodiamonds b) C1350 and c) C1700. (A color version of this figure can be viewed online.)

removal of the inter-particle bottlenecks amorphous carbon and a part of the outer shell of CNOs. For both C1350 and C1700, only a slight modification of SSA by hydrogen thermal treatment was observed (Table 1).

The pore size distribution (Fig. 3b) shows, for all materials, a pore size in the micropore region (~1 nm) and mesopores of about 10 nm, corresponding to the interparticles and inter-cluster spaces between the CNOs. However, the assignment of the pore size distribution to different “spaces” in the CNOs is much complex as highlighted recently elsewhere [51].

The surface chemistry and defects modifications induced by the air and hydrogen treatments were monitored by temperature programmed desorption coupled with mass-spectrometry. The material is heated under vacuum and the oxygenated groups present on the carbon surface are removed with the formation of CO and CO₂ gases. The release temperature of gases gives indication of their chemical nature [32]. Fig. 4a and b shows the CO₂ and CO desorption profiles of C1350 and C1700 and their corresponding modified materials after subsequent thermal oxidation under air and oxidation under air followed by hydrogen treatment.

Generally, CO₂ desorption occurs in the 150–700 °C temperature range, while CO desorbs at higher temperature between 320 and 950 °C (in-set Fig. 4a). The pristine CNOs i.e., C1350 and C1700 show low CO and CO₂ signals (Fig. 4a and b) suggesting a hydrophobic surface, with a low content in oxygenated groups. When treated under air, an intense CO desorption peak is observed in the high temperature range, i.e., 400–950 °C and 500–950 °C, for the C1350 and C1700 samples, respectively. This indicates the presence of basic oxygenated groups such as anhydrides, ethers, phenols or quinones [38,52–54].

It can be noticed as well that a small fraction of additional oxygenated groups could be formed on C1350 between 400 and 500 °C, which is related to the lower oxidation temperature (470 °C) compared to C1700 (580 °C). This can be well seen on the desorption peaks showing higher intensity for materials oxidized at

1350 °C.

In addition to CO desorption, CO₂ gas evolution is observed within the 400–600 °C temperature range mainly on the C1350 materials, suggesting the formation of acidic oxygenated groups such as anhydrides [38,52–54]. The intensity of the CO₂ peaks is significantly much lower than those of CO, showing that basic groups are predominantly formed on the materials by thermal oxidation. The hydrogenation treatment performed on these oxidized materials allows to remove the functional groups as shown by the low intensity CO and CO₂ profiles.

By integration of TPD-MS desorption curves, the amounts of desorbed CO and CO₂ groups can be determined as can be seen in Fig. 4c and Table 1. The calculated amounts well agree with the intensity of desorption profiles. The pristine materials C1350 and C1700 desorb very low quantities of CO_x (<0.1 mmol/g), while the oxidation greatly improves the functionalization of the CNOs (C1300-Tair, C1300-2Tair, C1700-Tair, C1700-2Tair), with desorbed surface groups contents ranging from 1.4 to 4.0 mmol/g. We note that the CO_x amounts desorbed increase for longer oxidation times and for the C1350 family materials which are more reactive. The hydrogen treatment allows to remove most of the groups (C1350-Tair-H2, C1700-Tair-H2); the desorbed quantities are low (from 0.1 to 0.3 mmol/g) but slightly higher than that of the pristine carbons (C1300, C1700).

After cleaning the CNOs surface by a treatment at 950 °C under vacuum (TPD) the surface defects concentration – active surface area is measured by chemisorption of oxygen at 300 °C overnight, followed by a TPD-MS analysis. The ASA values are shown in Fig. 4d and are also listed in Table 1.

The well graphitized C1700 sample contains only small amounts of surface functional groups and is also poor in defects with the lowest value of the ASA. This sample can therefore be considered as a reference sample, having no surface chemistry and structural defects. After oxidation under air, oxygenated groups were created on the C1700 carbon surface as can be seen from the TPD-MS

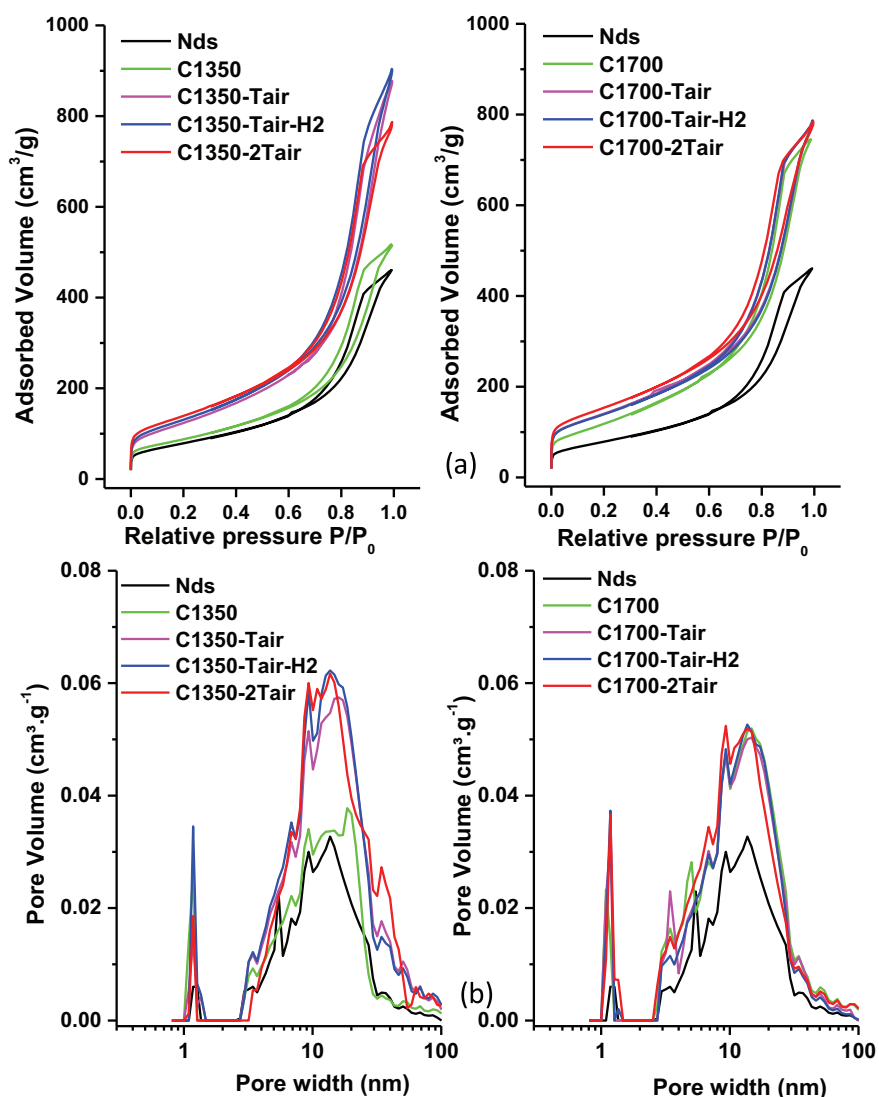


Fig. 3. (a) Nitrogen adsorption/desorption isotherms and (b) DFT pore size distribution of nanodiamonds, C1350 (left) and C1700 (right) carbons modified by different treatments. (A color version of this figure can be viewed online.)

Table 1
Specific surface area, amount of oxygen functional groups and active surface area values of CNOs treated under different conditions, and their corresponding capacitance in organic and aqueous electrolytes.

CNOs	SSA $\text{m}^2 \text{g}^{-1}$	$\text{DQ}_{(\text{CO}+\text{CO}_2)}$ mmol g^{-1}	ASA $\text{m}^2 \text{g}^{-1}$	ASA/SSA	C_{org} F/g	C_{aq} F/g
C1350	294	0.05	5	0.017	26	54
C1350-Tair	403	3	59	0.146	30	94
C1350-Tair-H2	433	0.3	49	0.113	31	79
C1350-2Tair	466	4	70	0.150	30	82
C1700	437	0.0	2	0.004	21	22
C1700-Tair	501	1.4	22	0.039	32	55
C1700-Tair-H2	466	0.1	17	0.037	30	41
C1700-2Tair	516	1.9	34	0.066	32	60

analysis (1.4 mmol g^{-1}). This step also led to the formation of defects ($\text{ASA} = 22 \text{ m}^2 \text{g}^{-1}$). Although further annealing under H_2 of this material allows removing most functional groups (0.2 mmol g^{-1}), very interestingly, the ASA is kept high ($17 \text{ m}^2 \text{g}^{-1}$). Considering the error of an ASA measurement (maximum 10%) these values can be considered similar. This result suggests a location of the functional groups in the defect sites; if not, the

removal of these groups would induce the formation of defects and therefore an increase in the ASA. Three different CNOs were thus obtained, with various surface chemistry and active sites: one sample (C1700) free of oxygenated groups and defects; a second sample (C1700-Tair) with oxygenated groups and defects and the third one (C1700-Tair-H2) with low oxygen groups content but with significant amount of defects. For the second series of C1350,

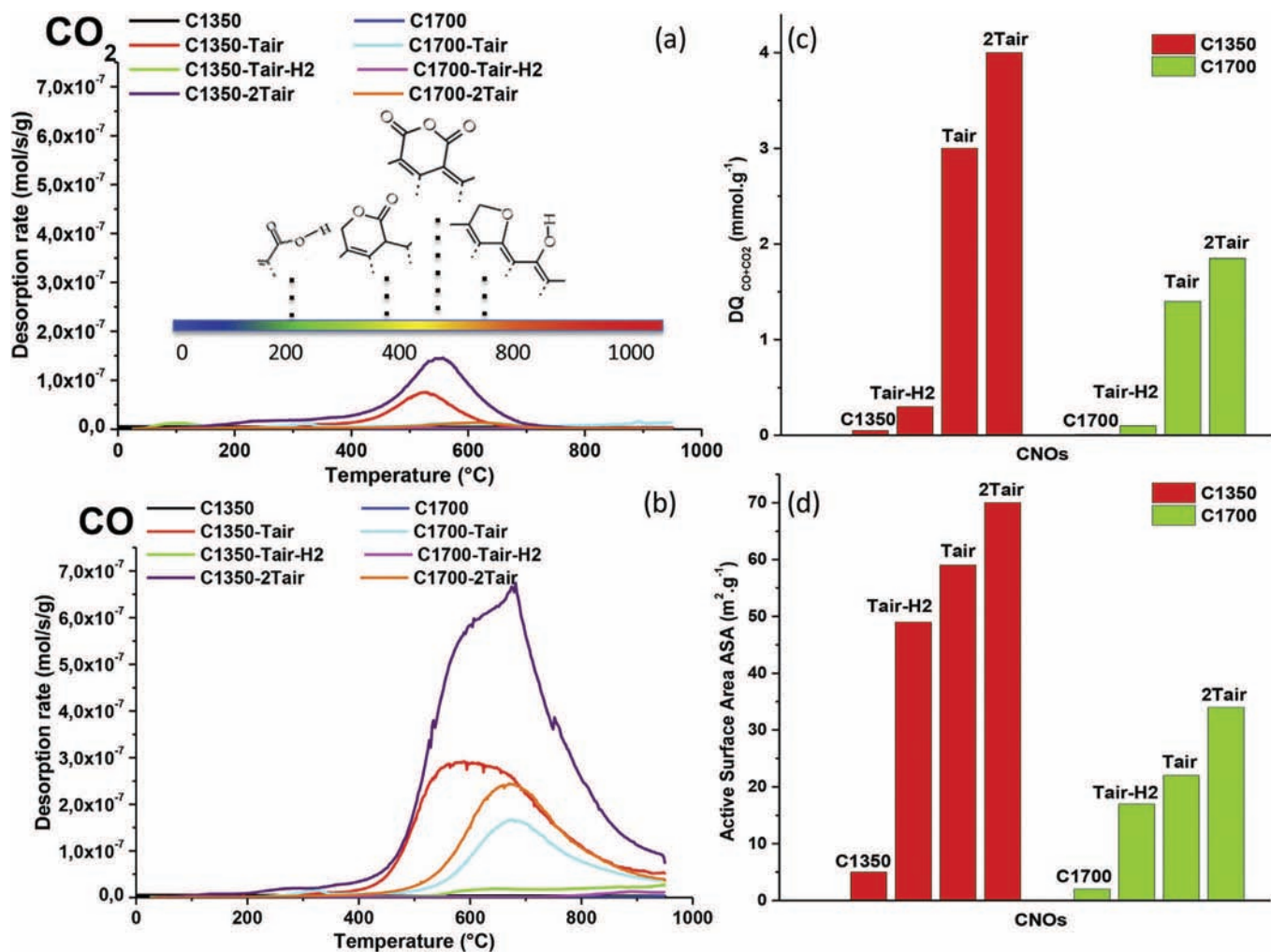


Fig. 4. TPD-MS desorption curves of a) CO₂ and b) CO along with the types of oxygen functional groups related to the CO and CO₂ desorption's profile c) Desorbed quantities of oxygen functional groups d) Active Surface Area of CNOs. (A color version of this figure can be viewed online.)

the same trend was observed but the experimental value shows that the amount of oxygenated groups and defects is three times higher than that of the C1700 series. Since the SSA area changes with these treatments, the ASA/SSA ratio was determined and we notice the same trend between the materials (Table 1).

These materials with distinct surface chemistry and defects contents will be used to understand the electrochemical performances of supercapacitors operating with different electrolytes.

The electrochemical performances of CNOs sample were determined in Swagelok cells in two-electrode configuration, in organic and aqueous electrolytes. Cyclic voltammograms at 20 mV s⁻¹ in 1.5 M NEt₄BF₄/ACN and 0.1 M H₂SO₄ are shown in Fig. 5a and b, respectively. All CVs exhibit a rectangular shape, which is characteristic of a capacitive behavior [24,44,55]. The peaks at 0.4 V and 0.8 V in aqueous electrolyte for CNOs1350 are associated with the pseudocapacitive contributions of surface functional groups [56–58].

The resulting gravimetric capacitance for all CNOs in both electrolytes as a function of desorbed CO and CO₂ quantities (DQ) are shown in Fig. 6. As a general trend, the capacitance increases with the amount of DQ for both CNOs series (Fig. 6 a and b). Since the amount of DQ is three times greater for the C1350 series than that of the 1700 series, therefore the capacitance is also three times higher. The maximum capacitance approaches 100 F/g, which is

higher than those reported before for such materials [4,7,26,30,31]. Aside, the increase in the capacitance is much pronounced in aqueous electrolyte than in organic electrolytes. This suggests more specific interactions between the oxygenated groups and the aqueous electrolyte, in agreement with the existence of pseudo-capacitive mechanism [59,60] in addition to the electric double layer capacitive behavior [56].

As pointed out by Macdonald et al. [61], interactions between adsorbed species depends on the Helmholtz free energy and the chemical potential. In other words, the capacitance associated with the adsorption is now assimilated to a new capacitance expressed as a “Langmuir” capacitance [61].

$$C(\theta) = q \cdot \left(\frac{z_i F}{RT} \right) \cdot \frac{\theta(1 - \theta)}{1 + r\theta(1 - \theta)} \quad (1)$$

where C is the capacitance, θ is the number of sites of the surface which are covered with gaseous molecules ($(1 - \theta)$ being the fraction of surface which is free from gas molecules), q is the charge corresponding to one monolayer, z_i is the charge of the ion and F is the faraday, r is the average pore radius. This is agreement with the trend curves represented in Fig. 6. All trend curves follow the Langmuir expression that we've cited before and their equation is assimilated to

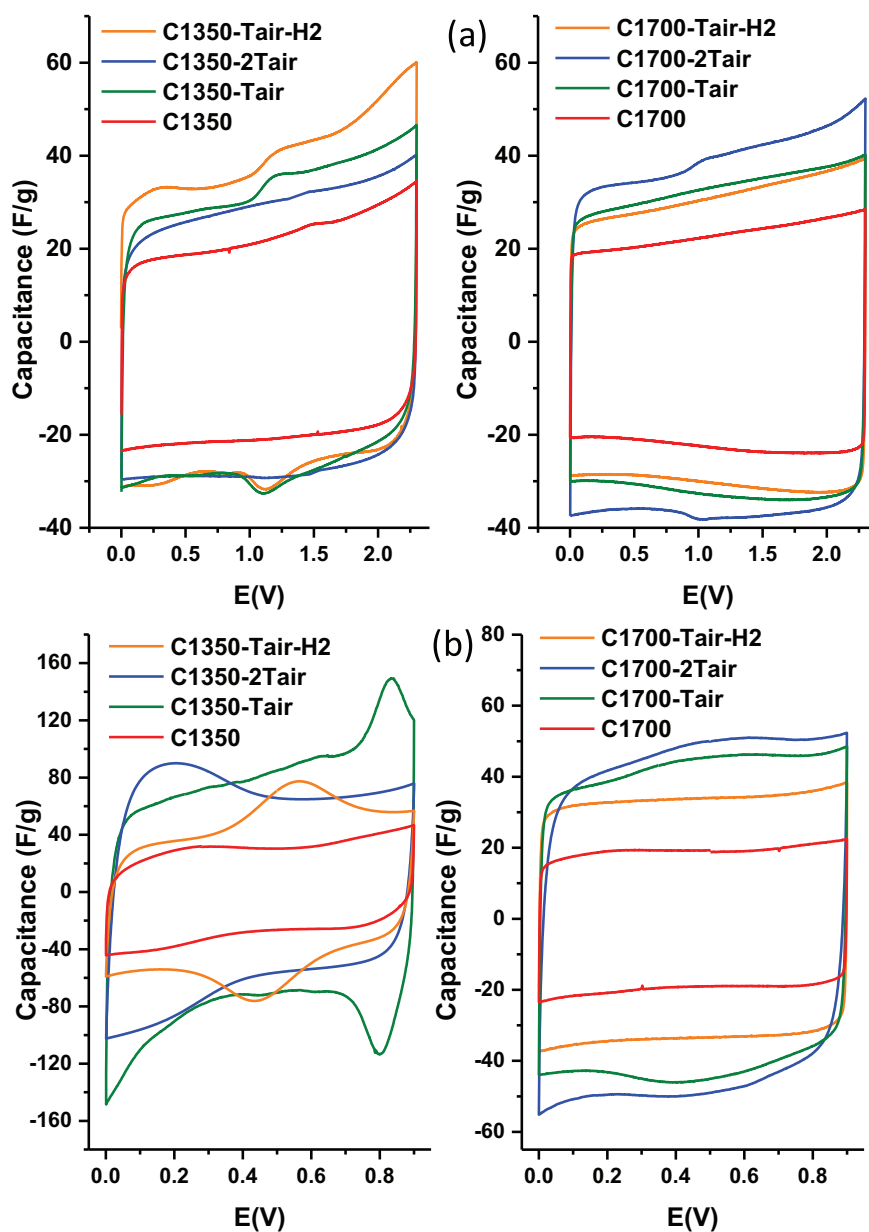


Fig. 5. Cyclic voltammetry curves of CNOs materials modified by different treatments at scan rate 20 mV s^{-1} using Swagelok assembling (2-electrodes) (a) in organic electrolyte (1.5 M NEt₄BF₄/AN) and (b) in aqueous electrolyte (0.1 M H₂SO₄). (A color version of this figure can be viewed online.)

$$y = \frac{a \cdot x}{1 + b \cdot x} \quad (2)$$

With the values of a and b are reported in Table 2.

This correlation is obtained for materials with similar characteristics in terms of SSA and surface chemistry (similar type of basic oxygen groups). However, by changing the process, different types/amounts of oxygen groups can be introduced onto the carbon sample surface (see Table S1 and Fig. S3) leading to an absence of any clear correlation between the capacitance in organic/aqueous electrolytes and the quantity of oxygen groups (see Fig. S4). This suggests the importance of the nature of the oxygen groups on the capacitance. Additional studies are needed to fully understand the influence functional groups nature on the capacitance response.

An important concern deals with the role of the defects (ASA) on the capacitance in both aqueous and organic electrolytes. Such

effect has not been studied in detail before. Fig. 7 shows the correlation between the capacitance and the ASA/SSA ratio, in aqueous and organic electrolytes. We notice that in aqueous and organic electrolytes, the capacitance for both CNO series (1350 and 1700) increases linearly with the increase of the ratio ASA/SSA. Similarly to the effect of DQ, the effect of ASA is greater for C1350 series and in aqueous electrolytes.

However, both the ASA and the surface functional groups (surface chemistry) changes for all the samples (see Table 1). To discriminate the influence of the presence of surface groups or the ASA on the capacitance, three samples have been prepared: C1700, C1700-Tair and C1700-Tair-H2. The results of the electrochemical tests are shown in Fig. 8.

C1700 and C1700-Tair-H2 samples exhibit similar low quantities of oxygenated groups ($<0.1 \text{ mmol/g}$, Table 1) but very different ASA (1.3 and $17 \text{ m}^2 \text{ g}^{-1}$ for C1700 and C1700-Tair-H2, respectively). The

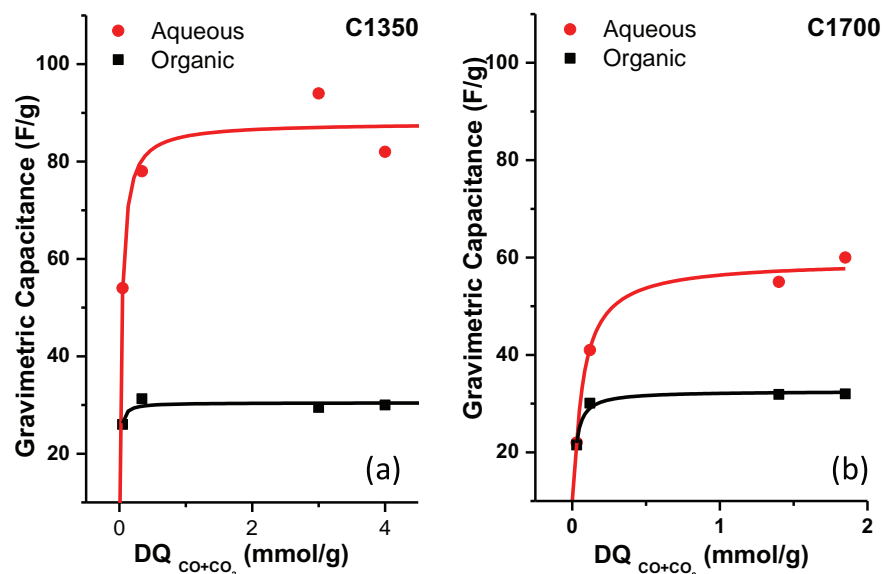


Fig. 6. The correlation between the capacitance and the desorbed quantities (DQ) of CO and CO₂ in aqueous and organic electrolytes for (a) C1350 and (b) C1700 carbons. (A color version of this figure can be viewed online.)

Table 2

Different values of a and b used in the expression of “Langmuir” capacitance to calculate the trend curves of the C1350 and 1700 carbon series in aqueous electrolyte (0.1 M H₂SO₄) and organic electrolyte (1.5 M NEt₄BF₄/AN).

Samples	a	b
C1350 series_Organic Elec.	3813	125
C1350 series_Aqueous Elec.	2715	31
C1700 series_Organic Elec.	2239	69
C1700 series_Aqueous Elec.	1134	19

g) mainly arises from the porosity (surface area). Differently, for the C1700-Tair-H2 sample with high ASA and low surface group content, the approx. 2-fold increase in capacitance (41 F/g) can be associated with the ASA increase. This clearly shows a major contribution of ASA to capacitance compared to functional groups.

C1700-Tair and C1700-Tair-H2 show similar high ASA values (22 and 17 m² g⁻¹ for C1700-Tair and C1700-Tair-H2, respectively) but different quantities of oxygenated groups (1.4 mmol/g and 0.1 mmol/g for C1700-Tair and C1700-Tair-H2, respectively). The capacitance was measured at 60 and 40 F/g for C1700-Tair and

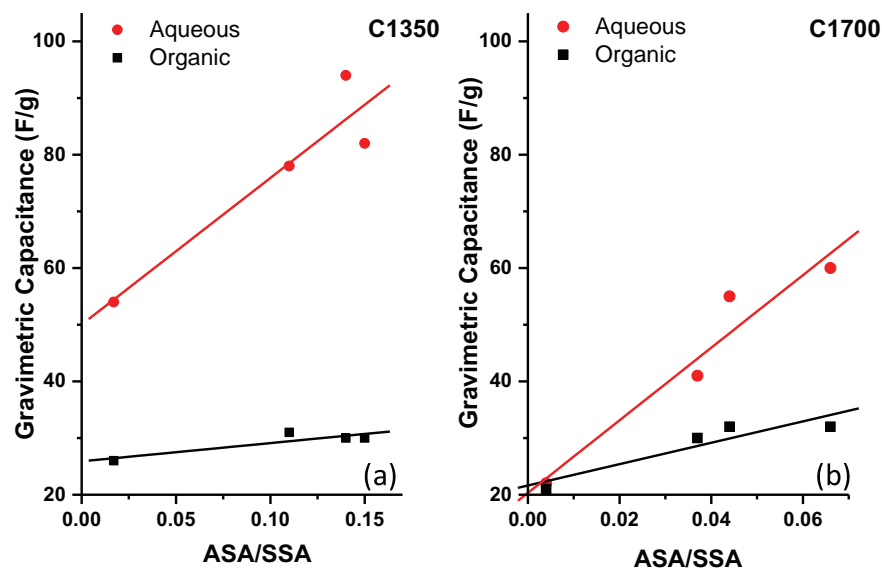


Fig. 7. The correlation between the capacitance and the ratio ASA/SSA in organic electrolytes (NEt₄BF₄/ACN) and aqueous electrolytes (H₂SO₄) for (a) C1350 and (b) C1700 carbons. (A color version of this figure can be viewed online.)

capacitance in aqueous electrolyte for the C1700 sample was measured at 22 F/g vs. 41 F/g for C1700-Tair-H2. Hence, since C1700 has low surface chemistry content and ASA, the capacitance (22 F/

C1700-Tair-H2, respectively). This suggests that the contribution of functional groups to the total capacitance in the C1700-Tair material is about 20 F/g, while the other 40 F/g comes from the porosity

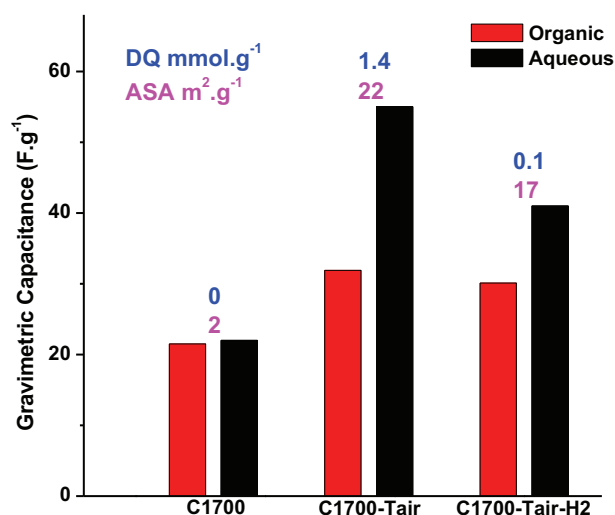


Fig. 8. Gravimetric capacitances of C1700 series in organic electrolytes ($\text{NET}_4\text{BF}_4/\text{ACN}$) and aqueous electrolytes (H_2SO_4) and their corresponding values in terms of desorbed quantities DQ and ASA. (A color version of this figure can be viewed online.)

and ASA. These results clearly show the important role of ASA in the capacitance improvement.

Similar behavior was seen for C1350, but higher capacitance values were obtained (95 F/g for C1350-Tair). To explain the improvement of the capacitance only by the presence of defects, we must consider that carbon atoms at the prismatic surface are more reactive than the basal plane atoms since they have an unpaired electron available to form bonds with oxygen [38]. In the case of graphitized carbon, the ASA represents essentially the reactivity of carbon edge planes. This means that the CNOs defects could interact with the aqueous electrolytes throughout oxygen bonds, allowing the improvement of interactions with the electrolyte and in consequence the capacitance behavior.

4. Conclusions

CNOs materials were synthesized from high-purity nanodiamonds and they underwent different types of thermal treatments in reducing or oxidizing atmosphere in order to modify their surface chemistry and their defects content (active sites). The proposed treatments allowed to finely tune the surface chemistry while keeping unchanged the amount of defects or inversely. For the first time, the precise control of these characteristics allowed highlighting a predominant influence of the carbon defects on the capacitance in organic and aqueous electrolytes which counterbalance the functional group effect. Hence, the functional groups have less influence on capacitance than usually stated and they influence more the CNOs performances in aqueous medium than organic one. These results bring new insights on the important characteristics of carbon to be improved in order to design new electrodes with high capacitance and energy density for supercapacitor applications. The extrapolation of these findings to commercially used activated carbon electrodes is of prime importance and will be discussed in our future works.

Acknowledgments

The Réseau sur le Stockage Electrochimique de l'Energie (RS2E) is acknowledged for financial support of this project through the ANR project Storex (ANR-10-LABX-76-01). The authors thank Joseph Denzter, Loïc Vidal, Jean-Marc Le Meins, Barbara Daffos and Wan-

Yu Tsai for their assistance with the TEM, TPD-MS, XRD and Cyclic Voltammetry measurements.

Appendix A. Supplementary data

Supplementary data related to this article can be found at <http://dx.doi.org/10.1016/j.carbon.2016.05.010>.

References

- [1] C. Liu, F. Li, L. Ma, H. Cheng, Advanced materials for energy storage, *Adv. Mater.* 22 (2010) 28–62.
- [2] F. Beguin, F. Frackowiak, *Carbons for Electrochemical Energy Storage and Conversion Systems*, CRC Press, New York, 2010.
- [3] P. Simon, Y. Gogotsi, Materials for electrochemical capacitors, *Nat. Mater.* 7 (2008) 845–854.
- [4] S. Candelaria, Y. Shao, W. Zhou, X. Li, J. Xiao, J. Zhang, Y. Wang, J. Liu, J. Li, G. Cao, Nanostructured carbon for energy storage and conversion, *Nano Energy* 1 (2012) 195–220.
- [5] B. Conway, *Electrochemical Supercapacitors: Scientific Fundamentals and Technological Applications*, Kluwer Academic Plenum Publisher, New York, 1999.
- [6] K. Kim, S. Park, Synthesis and high electrochemical capacitance of N-doped microporous carbon/carbon nanotubes for supercapacitor, *J. Electroanal. Chem.* 673 (2012) 58–64.
- [7] Q. Zhang, E. Uchaker, S. Candelaria, G. Cao, Nanomaterials for energy conversion and storage, *Chem. Soc. Rev.* 42 (2013) 3127–3171.
- [8] H. Helmholtz, Ueber einige Gesetze der Vertheilung elektrischer Ströme in körperlichen Leitern mit Anwendung auf die thierisch-elektrischen Versuche, *Ann. Phys.* 89 (1853) 211–233.
- [9] O. Mykhailiv, M. Imierska, M. Petelczyc, L. Echevoya, M. Plonska-Brzezinska, Chemical vs. electrochemical synthesis of carbon nano-onion/polypyrrole composites for supercapacitor electrodes, *Chem. Eur. J.* 21 (2015) 5783–5793.
- [10] F. Beguin, V. Presser, A. Balducci, E. Frackowiak, Carbons and electrolytes for advanced supercapacitors, *Adv. Mater.* 26 (2014) 2219–2251.
- [11] K. Makgopa, P. Ejikeme, C. Jafta, K. Raju, M. Zeiger, V. Presser, K. Ozoemena, A high-rate aqueous symmetric pseudocapacitor based on highly graphitized onion-like carbon/birnessite-type manganese oxide nanohybrids, *J. Mater. Chem. A* 3 (2015) 3480–3490.
- [12] J. Chmiola, G. Yushin, Y. Gogotsi, C. Portet, P. Simon, P. Taberna, Anomalous increase in carbon capacitance at pore sizes less than 1 nanometer, *Science* 313 (2006) 1760–1763.
- [13] C. Decaux, C. Matei-Ghimbeu, M. Dahbi, M. Anouti, D. Lemordant, F. Beguin, C. Vix-Guterl, E. Raymundo-Piñero, Influence of electrolyte ion-solvent interactions on the performances of supercapacitors porous carbon electrodes, *J. Power Sources* 263 (2014) 130–140.
- [14] G. Gong, Q. Xie, Y. Zheng, Y. Chen, S. Ye, Regulation of pore size distribution in coal-based activated carbon, *New Carbon Mater.* 24 (2009) 141–146.
- [15] I. Kim, M. Egashira, N. Yoshimoto, M. Morita, On the electric double-layer structure at carbon electrode/organic electrolyte solution interface analysed by ac impedance and electrochemical quartz-crystal microbalance responses, *Electrochim. Acta* 56 (2011) 7319–7326.
- [16] P. Liu, M. Verbrugge, S. Soukiazian, Influence of temperature and electrolyte on the performance of activated-carbon supercapacitors, *J. Power Sources* 156 (2006) 712–718.
- [17] R. Mysyk, E. Raymundo-Piñero, J. Pernak, F. Beguin, Confinement of symmetric tetraalkylammonium ions in nanoporous carbon electrodes of electric double-layer capacitors, *J. Phys. Chem. C* 113 (2009) 13443–13449.
- [18] E. Raymundo-Piñero, K. Kierzek, J. Machnikowski, F. Beguin, Relationship between the nanoporous texture of activated carbons and their capacitance properties in different electrolytes, *Carbon* 44 (2006) 2498–2507.
- [19] J. Segalini, E. Iwama, P. Taberna, Y. Gogotsi, P. Simon, Steric effects in adsorption of ions form mixed electrolytes into microporous carbon, *Electrochem. Comm.* 15 (2012) 63–65.
- [20] C. Vix-Guterl, E. Frackowiak, K. Jurewicz, M. Friebe, J. Parmentier, F. Béguin, Electrochemical energy storage in ordered porous carbon materials, *Carbon* 43 (2005) 1293–1302.
- [21] X. Zhang, R. Zhang, B. Xing, G. Cheng, Y. Xie, W. Qiao, L. Zhan, X. Liang, L. Ling, Effect of pore structure on the electrochemical performance of coal-based activated carbons in non-aqueous electrolyte, *New Carbon Mater.* 25 (2010) 129–133.
- [22] E. Calvo, N. Rey-Raap, A. Arenillas, A. Menendez, The effect of the carbon surface chemistry and electrolyte pH on the energy storage of supercapacitors, *RSC Adv.* 4 (2014) 32398–32404.
- [23] E. Frackowiak, Carbon materials for supercapacitors applications, *Phys. Chem. Chem. Phys.* 9 (2007) 1774–1785.
- [24] W. Tsai, P. Gao, B. Daffos, P. Taberna, C. Perez, Y. Gogotsi, F. Favier, P. Simon, Ordered mesoporous silicon carbide-derived carbon for high-power supercapacitors, *Electrochem. Comm.* 34 (2013) 109–112.
- [25] J. Chmiola, G. Yushin, Y. Gogotsi, C. Portet, P. Simon, P. Taberna, Anomalous increase in carbon capacitance at pore sizes less than 1 nanometer, *Science* 313 (2006) 1760–1763.

- [26] Q. Huang, D. Yu, B. Xu, W. Hu, Y. Ma, Y. Wang, Z. Zhao, B. Wen, J. He, Z. Liu, Y. Tian, Nanotwinned diamond with unprecedented hardness and stability, *Nature* 510 (2014) 250–253.
- [27] Y. Xia, Y. Zhu, Y. Tang, Preparation of sulfur-doped microporous carbons for the storage of hydrogen and carbon dioxide, *Carbon* 50 (2012) 5543–5553.
- [28] K. Jurewicz, K. Babel, A. Ziolkowski, H. Wachowska, Ammoxidation of active carbons for improvement of supercapacitor characteristics, *Electrochim. Acta* 48 (2003) 1491–1498.
- [29] H. Andreas, B. Conway, Examination of the double-layer capacitance of an high specific-area C-cloth electrode as titrated from acidic to alkaline pHs, *Electrochim. Acta* 51 (2006) 6510–6520.
- [30] C. Largeot, C. Portet, J. Chmiola, P. Taberna, Y. Gogotsi, P. Simon, Relation between the ion size and pore size for an electric double-layer capacitor, *J. Am. Chem. Soc.* 130 (2008) 2730–2731.
- [31] B. Garcia, S. Candelaria, G. Cao, Nitrogenated porous carbon electrodes for supercapacitors, *J. Mater. Sci.* 47 (2012) 5996–6004.
- [32] J.L. Figueiredo, M.F.R. Pereira, M.M.A. Freitas, J.J.M. Orfao, Modification of the surface chemistry of activated carbons, *Carbon* 37 (1999) 1379–1389.
- [33] J. Figueiredo, J. Sousa, C. Orgek, M. Pereira, J. Orfao, Adsorption of dyes on carbon xerogels and templated carbons: influence of surface chemistry, *Adsorption* 17 (2011) 431–441.
- [34] C. Matei Ghimbeu, R. Gadiou, J. Dentzer, D. Schwartz, C. Vix-Guterl, Influence of surface chemistry on the adsorption of oxygenated hydrocarbons on activated carbons, *Langmuir* 26 (2010) 18824–18833.
- [35] J.H. Zhou, Z.J. Sui, J. Zhu, P. Li, D. Chen, Y.C. Dai, W.K. Yuan, Characterization of surface oxygen complexes on carbon nanofibres by TPD, XPS and FT-IR, *Carbon* 45 (2007) 785–796.
- [36] M. Ismail, K. Ismail, Structure and active surface area of carbon fibers, *Carbon* (1987) 653–662.
- [37] P. Ehrburger, N. Puset, P. Dzedzinl, Active surface area of microporous carbons, *Carbon* 30 (1992) 1105–1109.
- [38] Bernardo Ph. J. Dentzer, R. Gadiou, W. Märkle, D. Goers, P. Novák, M.E. Spahr, C. Vix-Guterl, Influence of graphite surface properties on the first electrochemical lithium intercalation, *Carbon* 49 (2011) 4867–4876.
- [39] B. Zhang, C. Matei-Ghimbeu, C. Laberty, C. Vix-Guterl, J. Tarascon, Correlation between microstructure and Na storage behavior in hard carbon, *Adv. Energy Mater.* 6 (2016) 1501588.
- [40] C. Matei Ghimbeu, C. Decaux, P. Brender, M. Dahbi, D. Lemordant, E. Raymundo-Piñero, M. Anouti, F. Beguin, C. Vix-Guterl, Influence of graphite characteristics on the electrochemical performance in alkylcarbonate LiTFSI electrolyte for Li-ion capacitors and Li-ion batteries, *J. Electrochem. Soc.* 160 (2013) A1907–A1915.
- [41] E. Bushueva, P. Galkin, A. Okotrub, L. Bulusheva, N. Gavrilov, V. Kuznetsov, S. Moiseev, Double layer supercapacitor properties of onion-like carbon materials, *Phys. Status Solidi* 245 (2008) 2296–2299.
- [42] Y. Gao, Y. Zhou, M. Qian, X. He, J. Redepenning, P. Goodman, H. Li, L. Jiang, Y. Lu, Chemical activation of carbon nano-onions for high-rate supercapacitor electrodes, *Carbon* 51 (2013) 52–58.
- [43] C. Portet, G. Yushin, Y. Gogotsi, Electrochemical performance of carbon onions, nanodiamonds, carbon black and multiwalled nanotubes in electrical double layer capacitors, *Carbon* 45 (2007) 2511–2518.
- [44] J. McDonough, A. Frolov, V. Presser, J. Niu, C. Miller, T. Ubieto, M. Fedorov, Y. Gogotsi, Influence of the structure of carbon onions on their electrochemical performance in supercapacitor electrodes, *Carbon* 50 (2012) 3298–3309.
- [45] S. Tomita, T. Sakurai, H. Ohta, M. Fujii, S. Hayashi, Structure and electronic properties of carbon onions, *Chem. Phys.* 114 (2001) 7477–7482.
- [46] V. Kuznetov, A. Chuvilin, Y. Butenko, I. Malkov, V. Titov, Onion-like carbon from ultra-disperse diamond, *Chem. Phys. Lett.* 222 (1994) 343–348.
- [47] C. Matei-Ghimbeu, C. Decaux, P. Brender, M. Dahbi, D. Lemordant, E. Raymundo-Piñero, M. Anouti, F. Beguin, C. Vix-Guterl, Influence of graphite characteristics on the electrochemical performance in alkylcarbonate LiTFSI electrolyte for Li-Ion capacitors and Li-Ion batteries, *J. Electrochem. Soc.* 160 (2013) A1907–A1915.
- [48] Y. Gogotsi, P. Simon, True performance metrics in electrochemical energy storage, *Science* 334 (2011) 917–918.
- [49] M. Zeiger, N. Jackel, D. Weingarth, V. Presser, Vacuum or flowing argon: what is the best synthesis atmosphere for nanodiamond-derived carbon onions for supercapacitor electrodes? *Carbon* 94 (2015) 507–517.
- [50] V. Roddatis, V. Kuznetov, Y. Butenko, D. Sua, R. Schlogla, Transformation of diamond nanoparticles into carbon onions under electron irradiation, *Phys. Chem. Chem. Phys.* 4 (2002) 1964–1967.
- [51] M. Zeiger, N. Jackel, M. Aslan, D. Weingarth, V. Presser, Understanding structure and porosity of nanodiamond-derived carbon onions, *Carbon* 84 (2015) 584–598.
- [52] V. Ruiz, C. Blanco, E. Raymundo-Piñero, V. Khomenko, F. Béguin, R. Santamaria, Effects of thermal treatment of activated carbon on the electrochemical behaviour in supercapacitors, *Electrochim. Acta* 52 (2007) 4968–4973.
- [53] P. Brender, R. Gadiou, J.C. Rietsch, P. Fioux, J. Dentzer, A. Ponche, C. Vix-Guterl, Characterization of carbon surface chemistry by combined temperature programmed desorption with in situ X-ray photoelectron spectroscopy and temperature programmed desorption with mass spectrometry analysis, *Anal. Chem.* 84 (2012) 2147–2153.
- [54] C. Matei Ghimbeu, R. Gadiou, J. Dentzer, L. Vidal, C. Vix-Guterl, A TPD-MS study of the adsorption of ethanol/cyclohexane mixture on activated carbons, *Adsorption* 17 (2011) 227–233.
- [55] M. Plonska-Brzezinska, A. Molina-Ontoria, L. Echegoyen, Post-modification by low-temperature annealing of carbon nano-onions in the presence of carbohydrylates, *Carbon* 67 (2014) 304–317.
- [56] Y. Oh, J. Yooa, Y. Kima, J. Yoona, H. Yoona, J. Kima, S. Park, Oxygen functional groups and electrochemical capacitive behavior of incompletely reduced graphene oxides as a thin-film electrode of supercapacitor, *Electrochim. Acta* 116 (2014) 118–128.
- [57] M. He, K. Fic, E. Frackowiak, P. Novák, E.J. Berg, Ageing phenomena in high-voltage aqueous supercapacitors investigated by in situ gas analysis, *Energy Environ. Sci.* 9 (2016) 623–633.
- [58] V. Khomenko, E. Raymundo-Piñero, F. Béguin, A new type of high energy asymmetric capacitor with nanoporous carbon electrodes in aqueous electrolyte, *J. Power Sources* 195 (2010) 4234–4241.
- [59] H. Byon, S. Lee, S. Chen, P. Hammond, Y. Horn, Thin films of carbon nanotubes and chemically reduced graphenes for electrochemical micro-capacitors, *Carbon* 49 (2011) 457–467.
- [60] L. Lai, H. Yang, L. Wang, B. The, J. Zhong, H. Chou, L. Chen, W. Chen, Z. Shen, R. Ruoff, J. Lin, Preparation of supercapacitor electrodes through selection of graphene surface functionalities, *ACS Nano* 6 (2012) 5941–5951.
- [61] J. Macdonald, *Impedance Spectroscopy: Theory, Experiment, and Applications*, John Wiley and Sons, New York, 1987.